Magnetization reversal measurements in Gd/Fe multilayer antidot arrays by vector magnetometry using x-ray magnetic circular dichroism

D. R. Lee[a)]
Advanced Photon Source, Argonne National Laboratory, Argonne, Illinois 60439

Y. Choi
Advanced Photon Source, Argonne National Laboratory, Argonne, Illinois 60439 and Department of Materials Science and Engineering, Northwestern University, Evanston, Illinois 60208

C.-Y. You
Department of Physics, Inha University, Yonghyun-dong, Incheon 402-751, Korea

J. C. Lang, D. Haskel, and G. Srajer
Advanced Photon Source, Argonne National Laboratory, Argonne, Illinois 60439

V. Metlushko
Department of Electrical and Computer Engineering, University of Illinois at Chicago, Chicago, Illinois 60607

B. Ilic
School of Applied and Engineering Physics, Cornell University, Ithaca, New York 14858

S. D. Bader
Materials Science Division, Argonne National Laboratory, Argonne, Illinois 60439

(Received 13 June 2002; accepted 1 November 2002)

Fe K-edge x-ray magnetic circular dichroism (XMCD) was used as vector magnetometry to measure the magnetization rotation while field cycling Gd/Fe multilayer antidot arrays through a hysteresis loop. The measured XMCD hysteresis curves were then compared quantitatively with micromagnetic calculations to reconstruct the microscopic magnetization configurations. The best fit reveals the existence of three types of characteristic domains: two that rotate coherently during magnetization reversal and one that is strongly pinned. The behavior is explained by a simple three-domain energy model, including a phenomenological ansatz for a shape-induced demagnetization energy contribution. © *2002 American Institute of Physics.*
[DOI: 10.1063/1.1532552]

Patterning magnetic multilayers into dot arrays is of growing interest in high-density magnetoresistive random access memory and magneto-optic data storage media. However, there have been few studies of patterned ''antidot'' magnetic multilayers consisting of hole arrays in continuous magnetic films. Antidot arrays have recently received much attention because of their potential advantages over magnetic dot array systems for data storage.[1] Advantages include no superparamagnetic lower limit to the bit size and the preservation of the intrinsic properties of the continuous magnetic film. Antidot arrays possess unique magnetic properties, such as their shape-induced magnetic anisotropy, domain structure, and pinning in laterally confined geometries.[1–6]

For our first studies we chose antidot arrays of Gd/Fe multilayers. We focus on the regime in which Fe layers are decoupled at room temperature,[7,8] and study the magnetization reversal of Fe layers using element-specific x-ray magnetic circular dichroism (XMCD).[9] Future work will explore the influence of interlayer coupling on domain formation and switching of Fe and Gd layers. Typically, antidot arrays at remanence show three types of domains behaving collectively as single domains.[3–5] Domain formation at remanence is understood mainly as the result of the interplay between the intrinsic anisotropy and the shape anisotropy due to the antidots.[1–3,6] The coexistence of well-defined domains with individual magnetizations provides an opportunity to study the energetics between domains during magnetic switching. Here, we present XMCD as a vector magnetometry (VM) to understand the switching mechanism in antidot arrays. The approach is complementary to previous microscopy studies.[3–5] This work is also important for future studies of the interlayer coupling under lateral confinement because the element-specific XMCD technique is ideally suited for heteromagnetic systems such as Gd/Fe multilayers.

For the VM studies, hysteresis loops were measured by recording XMCD signals. Because XMCD is proportional to the projection of the magnetization vector $\mathbf{M}$ along the photon momentum direction $\hat{\mathbf{k}}_{\mathrm{ph}}$ near resonance energies [$\mathrm{XMCD} \propto \hat{\mathbf{k}}_{\mathrm{ph}} \cdot \mathbf{M} \approx |\mathbf{M}| \cos\gamma$, as shown in the inset of Fig. 1(a)], this technique allows element-specific determination of the orientation of the average magnetization. This is done by collecting hysteresis curves with more than two orthogonal incident photon directions for a given field.[10] Since XMCD-VM measures a spatially averaged magnetization, numerical micromagnetic simulations have been performed to reconstruct the microscopic domain configuration. The hysteresis loops were calculated using micromagnetic simu-

[a)]Electronic mail: drlee@aps.anl.gov

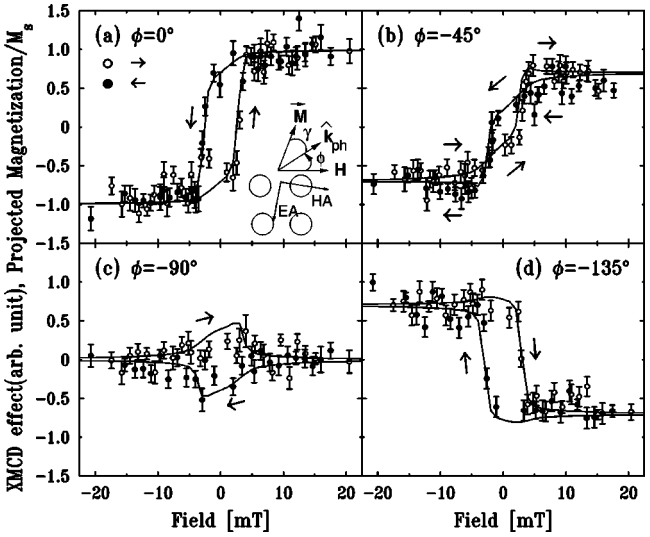

FIG. 1. XMCD magnetic hysteresis loops (circles) measured at the Fe K-edge at room temperature. To obtain vector information of the average magnetization, the incident photon beams were rotated with respect to the positive field direction by (a) $\phi=0°$, (b) $-45°$, (c) $-90°$, and (d) $-135°$. The inset in (a) shows a schematic of the experimental setup, where γ is the angle between the magnetization vector **M** and the incident photon momentum direction $\hat{\mathbf{k}}_{\mathrm{ph}}$, **H** is the applied field, and EA and HA denote the easy and hard axes of the intrinsic anisotropy, respectively. The solid lines represent the calculated hysteresis loops using micromagnetic simulations.

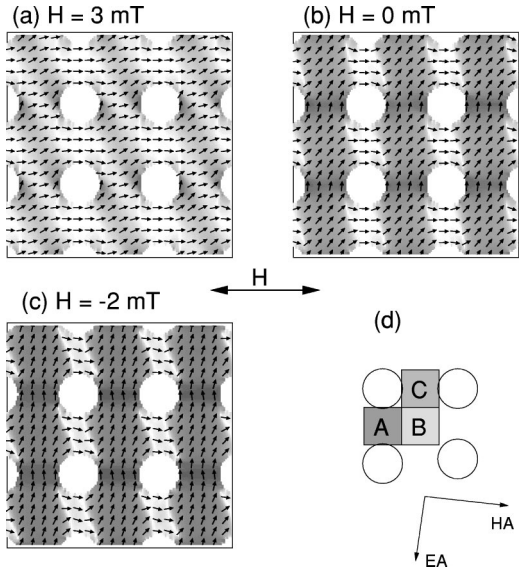

FIG. 2. The spin configurations of antidot arrays obtained from micromagnetic simulations with a sequence of applied fields of (a) 3 mT, (b) 0 mT, and (c) -2 mT. (d) Schematic of the three characteristic domains labeled A, B, and C in the unit cell.

lations and were fitted to the experimental data from XMCD-VM by varying the uniaxial anisotropy, exchange stiffness, and saturation magnetization as parameters. Our calculations resulted in a series of spin configurations showing coherent rotation of three types of domains. These coherent rotations are explained by a simple phenomenological energy model containing intrinsic uniaxial anisotropy and shape anisotropy induced by the antidots.

Multilayered $[\mathrm{Fe}(3\,\mathrm{nm})/\mathrm{Gd}(2\,\mathrm{nm})]_8$ films were prepared on Si substrates by e-beam deposition. Square arrays of circular holes with a period of 2 μm and a diameter of 1 μm were generated using standard lithography and lift-off processes. Magneto-optic Kerr effect (MOKE) hysteresis loops were measured for both unpatterned and patterned films to determine the direction of intrinsic uniaxial magnetic anisotropy. The XMCD measurements were performed at the SRI-CAT beamline 4-ID-D at the Advanced Photon Source. Circularly polarized hard x rays were produced by a diamond (111) quarter-wave plate operated in Bragg transmission geometry.[11] The XMCD effects were measured in fluorescence around the Fe K absorption edge (7.111 keV) by switching the helicity of the incident radiation. For the vector magnetometry studies, the sample/electromagnet assembly was rotated with respect to the projected incident photon direction.

Figure 1 shows XMCD hysteresis loops measured with four different directions of incident x-ray beams: (a) $\phi=0°$, (b) $-45°$, (c) $-90°$, and (d) $-135°$ with respect to the field applied in the positive direction. While $\phi=0°$ corresponds to the conventional hysteresis loop along the applied field direction, the rotation of the average magnetization of the sample at $\phi=-90°$ can be described by $\theta_{\mathrm{avg}}=-\tan^{-1}(M_{-90°}/M_{0°})$. This was surprising because one expected formation of many domains. Following this relationship, one can determine a counterclockwise rotation of magnetization from Figs. 1(a) and 1(c) induced by the easy-axis orientation of the intrinsic uniaxial anisotropy, as depicted by the inset in Fig. 1(a). The preferential rotation gives rise to a dramatic asymmetry between the $\phi=-45°$ and $\phi=-135°$ loops. Interestingly, $\phi=-45°$ hysteresis shows three loops whose tie points correspond to the coercive fields.

The microscopic domain configurations were reconstructed by comparing the measured XMCD hysteresis loops with calculated ones using micromagnetic simulations.[12] A uniaxial anisotropy constant $K_u=500\ \mathrm{J/m^3}$ was used for the best fit to the XMCD measurements, and typical values for Fe films were used for the other material parameters. The in-plane cell size was $20\times20\ \mathrm{nm}^2$, and the equilibrium configuration was assumed when the torque $|M\times H|/M_s^2 \leqslant 10^{-4}$. The thickness of the film was assumed to be 3 nm, corresponding to the individual Fe layer instead of the total thickness of Fe layers. To compare directly with the XMCD hysteresis loops in Fig. 1, average magnetizations projected along the directions with ϕ's were evaluated by $\langle \mathbf{M}_{\mathrm{cell}}(H)\cdot\hat{\mathbf{k}}_{\mathrm{ph}}(\phi)\rangle$. The fitted results from the two-dimensional code are shown as solid lines in Fig. 1, and are in good agreement with the measured XMCD hysteresis loops.

The reconstructed spin configurations with the best-fit parameters are shown in Fig. 2. The remanent domain structure in Fig. 2(b) clearly shows three main types of domains, as reported previously.[2,3] A sequence of spin configurations, as shown in Fig. 2, reveals that two types of domains, labeled as B and C in Fig. 2(d), rotate coherently, while one, labeled as A, is pinned. Figure 3 shows the magnetization orientations of these three types of domains obtained by collecting and averaging the cell magnetizations belonging to each types of domains from the micromagnetic simulations.

To understand intuitively the coherent rotations in Fig. 3, we have developed a simple phenomenological energy model by employing the Stoner–Wohlfarth single domain model with an effective shape anisotropy.[13] We assume that

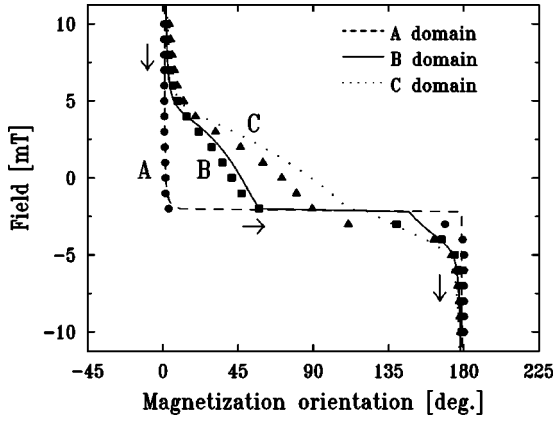

FIG. 3. Magnetization orientation of three types of domains depicted in Fig. 2(d) with respect to the positive field direction. The symbols represent the average value collected at each domain region from micromagnetic simulations, and the lines are calculated from the three-domain energy model.

the unit cell contains only *three* simple types of domains, labeled A, B, and C in Fig. 2(d), the magnetization orientations of which are defined by θ_A, θ_B, and θ_C, respectively. Further, we assume that the contributions of dipole interactions between each domain and domain wall energies at the boundaries are negligible. This is a valid assumption because when these effects are included, the final result is unchanged. The total magnetic energy density of the system is then given as:

$$E_{\text{tot}} = -\sum_{i=A,B,C} [M_s H \cos(\theta_i - \theta_H) + K_u \cos^2(\theta_i - \theta_E)] + E_{\text{shape}}, \quad (1)$$

where M_s is the saturation magnetization, H is the magnitude of the applied field and θ_H is its orientation, K_u is the intrinsic uniaxial anisotropy constant, and θ_E is the orientation of its easy axis. While the first and second terms in Eq. (1) represent the typical Zeeman and uniaxial anisotropy energies, respectively, E_{shape} is the total self-demagnetization energy (or the shape anisotropy, generally) ascribed to the antidot arrays. Since the free pole density is proportional to the component perpendicular to the boundary surface, E_{shape} can be expressed phenomenologically as:

$$E_{\text{shape}} = N_{\text{eff}} \frac{M_s^2}{2\mu_0} [\sin^2 \theta_A + (\cos \theta_A - \cos \theta_B)^2 + \cos^2 \theta_C + (\sin \theta_B - \sin \theta_C)^2], \quad (2)$$

where μ_0 is the permeability of free space, and N_{eff} is the effective demagnetization factor, which can be used as an adjustable parameter.

Substituting Eq. (2) into Eq. (1), the magnetization directions of each domain in static equilibrium can be obtained by the following conditions: $\partial E_{\text{tot}}/\partial \theta_i = 0$ and $\partial^2 E_{\text{tot}}/\partial \theta_i^2 > 0$. The solutions for θ_i were superimposed on the data from micromagnetic calculations, as shown in Fig. 3. In spite of the simplicity, the model shows reasonable agreement with micromagnetic results except for small discrepancies for the C-domain rotation and the coercive field. This strongly suggests that the interplay between the shape anisotropy and the intrinsic uniaxial anisotropy can explain the coherent rotations of domains as well as characteristic domain formations in antidot arrays. As the applied field decreases, while domain C starts to rotate to 90°, minimizing both shape and intrinsic anisotropy energy, domain A prefers to align to the field direction due to relatively stronger shape anisotropy exerted on it. A compromise between A and C domains leads to an energetically favorable domain configuration at remanence; that is, $\theta_A \sim 0°$, $\theta_B \sim 45°$, and $\theta_C \sim 90°$, as shown in Figs. 2 and 3.

In conclusion, by combining XMCD vector magnetometry measurements with micromagnetic simulations on antidot arrays, we determined that coherent rotations of magnetic domains occur during magnetization reversal. This is explained by a simple three-domain energy model. Future studies, combined with Gd L-edge XMCD measurements, on Gd/Fe antidot arrays will provide further insight into the lateral confinement effect on magnetically heterogeneous systems. Of further interest are antidot arrays with giant magnetoresistance and pseudospin valve structures.

We thank M. Grimsditch for MOKE measurement, and S.-B. Choe for helpful discussions. Work at Argonne is supported by the U.S. DOE, Office of Basic Energy Sciences, under Contract No. W-31-109-ENG-38. One of the authors (V.M.) is supported by the U.S. NSF, Grant No. ECS-0202780.

[1] R. P. Cowburn, A. O. Adeyeye, and J. A. C. Bland, Appl. Phys. Lett. **70**, 2309 (1997).
[2] L. Torres, L. Lopez-Diaz, and J. Iñiquez, Appl. Phys. Lett. **73**, 3766 (1998).
[3] A. Y. Toporov, R. M. Langford, and A. K. Petford-Long, Appl. Phys. Lett. **77**, 3063 (2000).
[4] C. T. Yu, J. Jiang, L. Shen, P. J. Flanders, and G. J. Mankey, J. Appl. Phys. **87**, 6322 (2000).
[5] U. Welp, V. K. Vlasko-Vlasov, G. W. Crabtree, C. Thompson, V. Metlushko, and B. Ilic, Appl. Phys. Lett. **79**, 1315 (2001).
[6] I. Guedes, N. J. Zaluzec, M. Grimsditch, V. Metlushko, P. Vavassori, B. Ilic, P. Neuzil, and R. Kumar, Phys. Rev. B **62**, 11719 (2000).
[7] R. E. Camley and D. R. Tilley, Phys. Rev. B **37**, 3413 (1988).
[8] D. Haskel, G. Srajer, J. C. Lang, J. Pollmann, C. S. Nelson, J. S. Jiang, and S. D. Bader, Phys. Rev. Lett. **87**, 207201 (2001).
[9] G. Schütz, W. Wagner, W. Wilhelm, P. Kienle, R. Zeller, R. Frahm, and G. Materilik, Phys. Rev. Lett. **58**, 737 (1987); C. T. Chen, Y. U. Idzerda, H.-J. Lin, G. Meigs, A. Chaiken, and G. A. Prinz, Phys. Rev. B **48**, 642 (1993).
[10] V. Chakarian, Y. U. Idzerda, G. Meigs, E. E. Chaban, J.-H. Park, and C. T. Chen, Appl. Phys. Lett. **66**, 3368 (1995).
[11] J. C. Lang and G. Srajer, Rev. Sci. Instrum. **66**, 1540 (1995).
[12] http://math.nist.gov/oommf
[13] E. C. Stoner and E. P. Wohlfarth, Philos. Trans. R. Soc. London, Ser. A **240**, 599 (1948).